Biventricular cardiac dynamic shape: genetics and cardiometabolic disease associations

Authors and affiliations

Richard Burns[1,2,3,4], William J. Young[2,3], Kulsuma Uddin[2], Steffen E Petersen[2,3,4], Julia Ramírez*[2,5,6], Alistair A Young*^[1], Patricia B Munroe*^[2,3,4]

1. School of Biomedical Engineering and Imaging Sciences, King's College London, London, UK
2. William Harvey Research Institute, Queen Mary University London, Charterhouse Square, London, UK
3. Barts Heart Centre, St Bartholomew's Hospital, Barts Health NHS Trust, West Smithfield, London, UK
4. NIHR Barts Biomedical Research Centre, Queen Mary of University London, Charterhouse Square, London, UK
5. Aragon Institute of Engineering Research, University of Zaragoza, Zaragoza, Spain
6. Centro de Investigación Biomédica en Red – Bioingeniería, Biomateriales y Nanomedicina, Zaragoza, Spain

*Indicates joint supervisors

^ indicates corresponding authors

Abstract

Background: Genetic studies using cardiac magnetic resonance (CMR) imaging have identified loci related to cardiac shape, but most focus on static morphology. The value of a dynamic cardiac shape atlas capturing both shape and function remains unknown.

Methods: A dynamic shape atlas comprising CMR-derived shape models at end-diastole and end-systole was combined with genetic and outcome data in 36,992 UK Biobank participants. Dynamic shape principal components (PCs) describing >1% of variance were characterized, and tested for associations with prevalent and incident cardiometabolic diseases, including ischemic heart disease (IHD), heart failure (HF), significant atrioventricular block (AVB), and atrial fibrillation (AF), and independent predictive power alongside standard CMR measures. Genome-wide association studies (GWAS) were performed to identify candidate genes and biological pathways, and polygenic risk scores (PRS) were assessed for disease associations. Mendelian randomization (MR) was performed to test causality of observed disease associations.

Results: We identified 14 dynamic cardiac shape PCs capturing 83.3% of total dynamic cardiac shape variance. These PCs captured distinct functional remodeling patterns such as variation in annular plane systolic excursion, while remaining only modestly correlated with standard CMR measures. All 14 PCs were associated with at least one incident cardiometabolic disease, with the strongest associations observed for incident IHD, HF, and AVB. Notably, incorporating dynamic shape PCs improved the prediction of incident IHD beyond standard CMR measures. GWAS identified 75 genetic loci associated with dynamic shape, including 14 variants previously unreported for cardiac traits, and candidate genes demonstrated enrichment in pathways related to cardiac development and contractile function. PRS derived from dynamic shape loci were significantly associated with multiple outcomes, most prominently HF. MR identified significant causal relationships between several PCs and cardiometabolic disease.

Conclusions: Dynamic cardiac shape features capture aspects of cardiac structure and function not fully represented by standard CMR measures. These features are strongly associated with incident cardiometabolic disease and provide new insights into the genetic architecture of cardiac remodeling.

Keywords: biventricular, dynamic cardiac shape and function, cardiometabolic disease, genome-wide association study

Clinical perspective:

What is new?

- Genetic and outcome relationships with a dynamic statistical shape model capturing both left and right ventricles at end-diastole and end-systole.
- Demonstration of incremental value over existing cardiac shape models, through capture of functional remodeling not represented by standard imaging measures.
- Identification of genetic susceptibility loci for dynamic cardiac shape, including 14 variants not previously reported for cardiac traits.

What are the clinical implications?

- The results enhance our understanding of the genetic architecture of dynamic cardiac shape and function in the general population and clarify their relationships with other cardiovascular endophenotypes and incident cardiometabolic diseases.
- Newly identified candidate genes expand the biological pathways implicated in cardiac remodeling and provide targets for future functional and mechanistic studies.
- The improved prediction of incident cardiometabolic disease, particularly ischemic heart disease, achieved by adding dynamic shape PCs to traditional CMR measures suggests potential value for their inclusion in evaluation of patients.

Introduction

The relationships between disease and cardiac morphology are bidirectional, in that disease can affect cardiac morphology through remodeling, and morphology can influence risk of cardiac disease incidence through physiological feedback mechanisms. For example, in ischemic heart disease (IHD) impaired blood flow may trigger myocardial remodeling, including hypertrophy or fibrosis[1–4], but pre-existing ventricular hypertrophy may conversely increase myocardial oxygen demand leading to ischemic conditions [5,6]. Cardiac structure and function measurements are therefore critical not only for diagnosing cardiovascular disease, but also for understanding disease risk mechanisms, pathogenesis, and prognosis[7,8]. However, standard measures such as ventricular volumes, masses, wall thicknesses, and ejection fraction do not capture all the morphological information present in modern cardiac imaging examinations.

Statistical cardiac shape atlas scores have established relationships with clinically meaningful measures[9–12], demonstrate stronger associations with prevalent disease than standard measures[11,13], and independently predict incident cardiovascular events[14]. However, the biological interpretation of the main drivers of shape variation, disease-shape relationships, and their genetic underpinnings remain limited. In particular, understanding the genetic basis of three-dimensional cardiac shape and motion may provide important insights into mechanisms underlying disease development.

Standard imaging-derived measures have a substantial genetic basis, including left and right ventricular end-diastolic (ED) and end-systolic (ES) volumes, myocardial mass, ejection fraction, myocardial strain, wall thickness, and sphericity[15–25]. Polygenic risk scores (PRS) derived from these traits have shown predictive value for cardiometabolic diseases, including cardiomyopathies[26–28], heart failure[29,30], atrial fibrillation[31–33], and type 2 diabetes mellitus[31,34,35]. More complex imaging-derived phenotypes have further expanded locus discovery, including regional wall thickness[25,36], trabecular complexity quantified by fractal dimension[37], and latent phenotypes derived from machine learning approaches[38–40]. Our previous work demonstrated that ED biventricular shape atlas scores have a significant genetic basis, with 43 associated loci[41]. However, analysis of coupled ED-ES shape and function, which utilizes information across the cardiac cycle and can better capture associations with cardiac functional disease, remains unexplored.

In this study, we investigated the relationships between a dynamic shape atlas, combining ED and ES shape in both left and right ventricles[42], and both prevalent and incident cardiometabolic disease in 36,992 participants of the UK Biobank, and evaluated the additive value of these phenotypes beyond standard measures in predictive models. We performed genome-wide association studies (GWAS), gene-burden testing, and downstream bioinformatic analyses to characterize the genetic basis of

dynamic cardiac shape and compared findings with our previously published ED-only shape GWAS[41]. We constructed PRS and conducted Mendelian randomization (MR) analyses to explore potential causal relationships between genetically determined shape variation and cardiometabolic disease. We hypothesized that dynamic cardiac shape phenotypes capture complementary structural and functional information that enables identification of novel loci, provides insight into cardiac remodeling mechanisms, and improves prediction of incident cardiometabolic disease beyond standard imaging measures.

Methods

Data availability

All UK Biobank (UKB) data are available upon application (www.ukbiobank.ac.uk). Summary GWAS statistics will be publicly available through the GWAS catalog (https://www.ebi.ac.uk/gwas) on publication.

Study population and cardiac phenotyping

UK Biobank is a large prospective cohort of approximately 500,000 participants aged 40-69 years at recruitment, with extensive demographic, clinical, lifestyle, and genetic data. Genotype data were available for 488,377 individuals, generated using the UK BiLEVE and UK Biobank Axiom arrays. Study design, genotyping, and quality control procedures have been described previously[43,44].

This study included cardiovascular magnetic resonance (CMR) imaging data from 45,683 participants, which has been described previously[45]. Briefly, images were acquired on a 1.5T wide-bore scanner (MAGNETOM Aera, Siemens Healthcare) using ECG-gating. Short-axis cine images covered both ventricles with 8 mm slice thickness and 2 mm inter-slice gap (TR=2.6msec, TE=1.10msec), interpolated to 50 phases per cardiac cycle. Long-axis cine images (2-, 3-, and 4- chamber views) were acquired with 6 mm slice thickness (TR 2.7 ms, TE 1.16 ms).

Image analysis and dynamic shape atlas construction

The automated image analysis and shape atlas pipeline has been described previously[42]. Briefly, short- and long-axis cine images were analyzed using Circle cvi42 (version 5.11 1505, Circle Cardiovascular Imaging Inc., Calgary, Canada), using deep learning convolutional neural networks to segment left ventricular (LV) endocardial and epicardial surfaces and right ventricular (RV) endocardial surfaces. Valve landmarks for the mitral, tricuspid, and aortic valves were also automatically extracted from long-axis views.

Biventricular subdivision surface meshes were generated at ED and ES using a non-rigid diffeomorphic registration framework[46]. Short- and long-axis contours were first aligned to correct for breath-hold misregistration, after which a template mesh was iteratively deformed to minimize contour-to-surface distances while preserving diffeomorphic properties.

A statistical shape atlas was constructed by aligning ED meshes using generalized Procrustes alignment[47] (excluding scaling to preserve size variation). The same transformation was applied to both ED and ES meshes, preserving individual-specific ED-ES displacement patterns. ED and ES were concatenated into a single vector per individual, and principal component analysis (PCA) was applied. Fourteen dynamic cardiac shape PCs explaining >1% of total variance each (83.3% cumulative variance) were retained, capturing joint morphological and functional variation across the cohort.

Shape quality control

Quality control procedures were performed to exclude cases in which the shape modeling process failed, as described previously[42]. Briefly, cases with incomplete information needed to construct a 3D shape model were excluded. Outlier shape models (chamber volumes exceeding 5 IQR) at ED or ES were excluded prior to PCA. After PCA, shape score outliers exceeding 3 IQR in Mahalanobis distance were excluded, and models with residual distance between the model surface and the PCA representation exceeding 3 IQR were excluded.

Associations with conventional CMR measures and ED shape atlas

To assess relationships between dynamic shape PCs and standard CMR-derived measures, Pearson correlations were computed for left and right ventricular volumes, masses, and ejection fractions. Associations between dynamic shape PCs and cardiometabolic disease risk factors were calculated similarly. Correlations with previously reported ED-only shape PCs[41] were also calculated to compare static and dynamic atlases. Analyses were performed in R (version 4.3.1).

Disease association analyses

Associations between dynamic shape PCs and cardiometabolic disease were assessed for six well-represented cardiometabolic diseases encompassing the different aspects of cardiac pathology in the UK Biobank: atrial fibrillation (AF), significant atrioventricular block (AVB), heart failure (HF), IHD, stroke, and type 2 diabetes (T2D). Multivariable logistic regression was used for prevalent disease and Cox proportional hazards models for incident disease. Covariates, selected through stepwise regression, included age at imaging, sex, height, body mass index (BMI), systolic and diastolic blood pressure (averaged between automated and manual readings and adjusted for medication use), serum high-density cholesterol (HDL), low-density lipoprotein (LDL) and mean triglyceride levels, smoking and alcohol consumption (*Supplementary Table 1*). Missing covariate data were imputed

using the MICE[48], version 3.16.0) imputation package in R. Significant associations were defined at P < 0.0083 (Bonferroni corrected at 0.05/6 diseases tested). Disease information was obtained from hospital episode statistics data through UKB. ICD9, ICD10 and OPCS-4 codes were used to define each disease (*Supplementary Table 2*). Prevalent and incident disease were defined using the date of each participant's CMR imaging and the date of disease diagnosis.

Incident disease prediction: contribution of dynamic shape PCs beyond standard CMR measures

We tested whether incorporating dynamic cardiac shape PCs alongside standard CMR measures improves prediction of incident cardiometabolic disease compared with models based on standard CMR measures alone. Cox proportional hazards regression was used to construct two models for each outcome.

The baseline model included standard CMR measures (left and right ventricular ED and ES volumes, myocardial masses, ejection fractions, stroke volumes, and global circumferential and longitudinal strain), together with established clinical covariates: sex, age, height, BMI, SBP and DBP, smoking status, alcohol consumption, serum HDL, LDL and triglyceride levels. The extended model included dynamic cardiac shape PCs in addition to the CMR measures and covariates retained from the baseline model.

Separate prediction cohorts were defined within UK Biobank for each cardiometabolic outcome (AF, AVB, HF, IHD, stroke, and T2D). Participants with a diagnosis of the relevant disease prior to their UK Biobank imaging assessment date were excluded. Incident disease was defined using linked electronic health record ICD codes (*Supplementary Table 2*).

A penalized Cox proportional hazards regression model framework with elastic net regularization within R glmnet[49,50] was used to model time to event for incident cardiometabolic diseases with equal lasso and ridge penalties to balance variable selection and coefficient shrinkage. The optimal regularization parameter was selected using internal cross-validation within the training data. Two models were created; the first a CMR model which combined clinical covariates identified to be significantly associated with each disease through stepwise regression (*Supplementary Table 1*) and CMR measures; and the second with these same variables as well as dynamic cardiac shape PCs. Model performance was assessed using five-fold cross validation, calculating predictive performance using concordance index (C-index). C-index variability, non-parametric bootstrap resampling was performed (with 1,000 samples), and the 95% confidence intervals are reported alongside the C-index.

Genetic analyses

A more detailed description of genetic analyses can be found in *Supplementary Methods*. Heritability of dynamic shape PCs was estimated in 36,992 unrelated white European participants with high-quality imaging data, no previous history of major cardiovascular disease, and a left ventricular ejection fraction of >40%, using BOLT-REML[51] version 2.3. GWAS were performed for each PC using a linear mixed model method (BOLT-LMM[52], version 2.4.1), testing 558,994 variants (minor allele frequency ≥1% and INFO >0.3), adjusting for age, sex, height, BMI, blood pressure, heart rate, array type and the top 10 genetic principal components. Genome-wide significance was defined as $P < 5x10^{-8}$. A genomic signal was defined as the most significant (lead) SNV and all SNVs within a 1mb window in linkage disequilibrium (LD) $r^2 > 0.1$. Population stratification and confounding were assessed using LD score software (LDSC)[53], v1.0.1. Secondary signals were identified using GCTA conditional analysis[54], version 1.94.1.

Functional annotation and pathway analyses

Candidate genes were prioritized using variant effect prediction (VEP)[55–57], expression quantitative trait locus (eQTL) colocalization analysis[58], transcriptome-wide association studies[59], Hi-C long-range chromatin interactions[60–62], Polygenic Priority Score (PoPS)[63], literature review, and mouse knockout phenotypes (*Supplementary methods*)[64]. Candidate genes were queried using Functional Mapping and Annotation of Genome-Wide Association Studies (FUMA GWAS)[65] to perform functional enrichment analysis. Significant enrichment was defined as an adjusted False Discovery Rate $P < 0.05$.

Rare variant analysis

We used Regenie[66] (v4.0) to assess the contribution of rare genetic variants to dynamic cardiac shape PCs, and prespecified variant masks and annotations were used. Leave one variant out (LOVO) analysis was performed to assess whether significant results were driven by single or multiple rare variants (*Supplementary methods*).

Genetic relationship with end-diastolic shape atlas

We assessed the genetic correlation between the dynamic cardiac shape atlas and previously published end-diastolic shape atlas using the software tool LDSC[53] (v1.0.1). All dynamic cardiac shape lead variants and high LD proxies ($r^2 > 0.8$) were also searched within the summary statistics of the end-diastolic shape GWAS, and results of variants with the lowest P-value among the 11 end-diastolic PCs are reported and shared signals across the cardiac atlases are indicated.

Pleiotropy and PheWAS analyses

To assess novelty of the EDES GWAS results and identify which genetic signals were not previously reported for cardiovascular traits, we collated a list of all genome-wide significant variants and high LD proxies ($r^2 > 0.8$) from a literature review of cardiac trait (cardiovascular diseases, electrocardiogram and measures of cardiac structure and function) GWAS and in the GWAS Catalog[67]. If an EDES GWAS lead variant was within 500kb of a previously reported SNV associated with a cardiovascular trait, and is in LD $r^2 \geq 0.1$, the association is reported.

We performed a phenome-wide association study (PheWAS) using the R package PheWAS[68] (version 0.99.6.1) to assess relationships between dynamic cardiac shape PC variants and curated phecodes for clinical conditions (only including case numbers ≥200), and to test PRS for these PCs with the same phecodes. The analysis was performed on UK Biobank individuals not included in the GWAS, and was adjusted for age, sex and the first 10 genetic principal components. A Bonferroni corrected threshold (number of phecodes tested 0.05/325 = 1.54×10^{-4}) was used to declare significance.

Polygenic risk scoring

We used PRSice-2[69] (version 2.3.5) to calculate each PRS, summing the dosage of each dynamic cardiac shape lead variant allele weighted by effect size (from GWAS) in the full UK Biobank genotyping cohort of 487,409 individuals. Associations were calculated through logistic regression of standard deviation increase in standardized PRS against cardiometabolic disease incidence in 447,408 unrelated (kinship pairs < 0.0884) individuals not included in the GWAS cohort. Disease outcomes were AF, AVB, HF, IHD, stroke and T2D (*Supplementary Methods*). Logistic regression models were adjusted for covariates identified to be significant for each disease through stepwise regression, selecting from age, sex, height, BMI, alcohol consumption, systolic and diastolic blood pressures, smoking status, LDL and mean triglyceride levels (*Supplementary Table 1*), the genetic array used and the first 15 genetic principal components. For the analysis the first visit covariate data was used. A P-value threshold of 0.00833 was used to define significant associations (Bonferroni corrected 0.05/number of diseases).

Mendelian Randomization

To explore the directionality and potential causality underlying significant associations between dynamic cardiac shape PCs and cardiometabolic diseases, Mendelian randomization (MR) analyses were performed using the TwoSampleMR[70] R package (version 0.6.6). PC-disease pairs selected for MR were based on statistically significant associations identified in regression analyses of dynamic shape PCs with prevalent and/or incident disease (*Supplementary methods*).

For associations with prevalent disease, where disease-related remodeling could influence cardiac shape, MR analyses were conducted with disease status as the exposure and dynamic cardiac shape PCs as the outcome. Conversely, for associations with incident disease, where cardiac shape may confer risk of future disease, MR analyses were performed with dynamic cardiac shape PCs as the exposure and disease incidence as the outcome. Additional methodological details, including instrument selection, sensitivity analyses, and assessment of pleiotropy and heterogeneity, are provided in the *Supplementary methods*.

Results

An overview of the study design is shown in *Figure 1*, with demographic details of the imaging and full UKB cohorts provided in *Table 1*. Of 45,683 individuals with suitable CMR images, 41,659 passed shape quality control and were included in the dynamic cardiac shape atlas. Fourteen PCs, each explaining > 1% of total variance were retained, jointly accounting for 83.3% of overall shape variability (*Table 2*). Genetic and shape data were available in 36,992 participants with complete covariate data.

Since PCA is an unsupervised dimension reduction method, individual PCs are not directly interpretable in terms of traditional measures. However, visual inspection of the PCs revealed that most can be associated with biologically interpretable patterns of cardiac structure and function (*Figure 2*). PC1 reflected overall heart size and was the dominant source of morphological variation in the population, consistent with the absence of size correction during Procrustes alignment[47]. Subsequent PCs therefore captured dynamic shape variation independent of global size. We observed several PCs that reflect functional remodeling: PC2 (10.62% variance) was associated with systolic excursion of the mitral and tricuspid annular planes (MAPSE/TAPSE); PC9 (2.08%) was related to LV basal systolic excursion; PC13 (1.14%) represented global biventricular ejection fraction and PC14 (1.04%) reflected variation in relative ventricular size and ejection fraction. These interpretations are summarized in Table 2, Figure 2, and can be further visualized in *Supplementary Movies 1-42*.

Relationships with standard CMR measures, cardiovascular risk factors and biventricular ED shape atlas

Correlations between dynamic shape PCs and standard CMR measures demonstrated both shared and complementary information (*Supplementary Figure 1*). PC1 showed strong correlations with volumetric measures and LV mass (r = 0.88-0.95). In contrast, function-related PCs exhibited only moderate or weak correlations with standard metrics. PC13 (biventricular ejection fraction) correlated moderately with LVEF and RVEF (r = -0.49 and -0.44), while PC2 (MAPSE/TAPSE) showed

weak correlations (r = 0.18 and 0.15) with LVEF and RVEF, indicating that dynamic shape features capture aspects of function not fully represented by standard CMR measures

Associations with cardiometabolic risk factors were heterogeneous (*Supplementary Figure 2*). PC1 was strongly associated with sex and age (r = 0.73 and 0.72), whereas several PCs, such as PC9 (LV basal systolic excursion) showed weaker relationships with classical risk factors (r<0.3), indicating that established epidemiological factors do not explain variation in biventricular shape and motion.

Comparisons with our previously published ED shape atlas[41] showed high concordance for size-related PCs (PC1, r = 0.98) and moderate correlations for selected geometric features (*Supplementary Figure 3*). In contrast, key functional PCs (e.g. PC2 and PC13) showed weak correlations with ED-only PCs, confirming that the dynamic atlas captures additional information derived from systolic deformation.

Associations with cardiometabolic diseases

Dynamic shape PCs were significantly associated with all six prevalent cardiometabolic diseases (*Supplementary Table 3*) after Bonferroni correction (*Figure 3*). Multiple PCs were associated with prevalent IHD, AF, and HF, often with patterns of risk-increasing and protective effects consistent with clinical expectations. Associations were also observed for AVB and T2D.

For incident outcomes, five diseases showed significant associations, excluding stroke (*Figure 3, Supplementary Table 4*). Interestingly, 13 PCs were associated with incident AVB, all in a risk-increasing direction. Several PCs showed discordant directions of association between prevalent and incident disease, consistent with a distinction between disease-related and shape-mediated disease susceptibility.

Functionally interpretable PCs showed particularly strong effects. Increased systolic annular excursion (PC2) was protective for prevalent IHD (OR 0.71, CI 0.67-0.74) but strongly associated with increased risk of incident IHD (HR 3.01, CI 2.64-3.42). Similarly, reduced ejection fraction captured by PC13 and PC14 was associated with markedly increased risk of incident HF and IHD (*Figure 3*).

Modeling incident cardiometabolic disease risk prediction

Inclusion of dynamic shape information from PC2 (valve annular plane systolic excursion) improved prediction accuracy of time to event for incident IHD beyond standard CMR and clinical measures alone (C-index 0.67 [CI 0.66-0.68], 0.63 [CI 0.62-0.64] respectively). The combined model includes PC2 alongside sex, age, SBP, HDL levels, LVESV, $LVM_{systolic}$ and global longitudinal strain measured in both the 3 and 4 chamber views. The accuracy for predicting time to incident diabetes also improved when including PC2 in a model alongside BMI and triglyceride levels (C-index 0.65 [CI 0.63-0.67]),

where the CMR model selected BMI, triglyceride levels, HDL levels and right ventricular septal global circumferential strain (C-index 0.59 [CI 0.56-0.61]). Cox regression models for predicting time to incident AF, stroke and AVB failed to meaningfully predict time to event with either model. The model for HF did not include dynamic shape information as a predictor in the final model. Variables selected for all models are reported in *Supplementary Table 5.* Results for all models are reported in *Supplementary Table 6*.

Genetic architecture of dynamic cardiac shape

All 14 PCs were heritable (h^2 = 12.3-36.9%, *Supplementary Table 7*). GWAS identified 75 genome-wide significant loci across the PCs (Table 3, Figure 4), with minimal evidence of confounding (λ = 1.05 - 1.15). Manhattan, locus zoom, and QQ plots are available in *Supplementary Figures.* Genetic correlations among PCs were modest to moderate (*Supplementary Table 8*), reflecting partially shared but distinct genetic influences.

Comparison with ED shape GWAS demonstrated substantial overlap for size and geometry-related PCs, but limited genetic correlation for functional PCs such as PC2 (MAPSE/TAPSE) and PC13 (ejection fraction (*Supplementary Table 9)*. Of the 77 lead signals (two independent signals at discovered loci), 20 were genome-wide significant in the ED shape GWAS, and 13 demonstrated suggestive significance ($5x10^{-8} < P < 1x10^{-6}$). Thirty lead signals were $1x10^{-6} < P < 1x10^{-3}$ and 14 had nominal significance $1x10^{-3} < P < 0.05$ (*Supplementary Table 10)*. Moreover, of the 77 lead signals, 14 of which had not previously been implicated in cardiac traits, and 8 were entirely novel across published GWAS at time of analysis (*Supplementary Table 11, Supplementary Table 12*).

Functional annotation identified two non-synonymous missense variants, one was predicted to be possibly damaging with PolyPhen (rs2234962, chr10:121429633:T>C, *BAG3,* PCs 1, 10 and 13) and one was predicted to be probably damaging (rs26821, chr5:102520400:A>G, *PPIP5K2*, PC7) (*Supplementary Table 13*). Twenty-two variants were identified as eQTLs in aortic artery, coronary artery, left ventricle and atrial appendage tissues[71], of which twenty had support for colocalization (PP4 > 0.75)[58] (*Supplementary Table 14*). Transcriptome-wide analysis identified 103 genes ($P < 3.1 \times 10^{-6}$, Bonferroni corrected) mapping to the boundaries of 40 loci (*Supplementary Table 15*). Finally, 280 Hi-C interactions were identified at 45 of the lead GWAS variants, summarized in *Supplementary Table 16*. Integrative gene prioritization including those genes identified by the aforementioned tools alongside results from PoPs, identified 77 candidate genes (*Supplementary Table 17*), enriched for pathways related to cardiac development ($P_{adj} = 2.79x10^{-5}$), muscle structure ($P_{adj} = 3.53x10^{-4}$), contractile function ($P_{adj} = 4.45x10^{-4}$, *Supplementary Table 18*).

Rare variant burden testing implicated established cardiomyopathy genes (e.g. *TTN for PC1, FHOD3 for PC10)*, providing convergent evidence with common variant findings (*Supplementary Table 19*). Five additional genes not identified in the common-variant GWAS showed evidence of rare variants driving associations ($P < 2.79x10^{-6}$); *RBM20* and *VPS25* for PC1 (overall heart size), *SMARCAD1* for PC3 (ventricular sphericity), *NKAPD1* for PC7 (septal position), *CSRP3* for PC14 (relative ventricular size and ejection fraction). There was significant evidence that multiple rare missense variants were driving the associations at *TTN* and *SMARCAD1* (*Supplementary Table 19*).

Polygenic risk and causal inference

PRS derived from dynamic shape PCs were associated with a broad range of cardiovascular phenotypes in PheWAS, predominantly within the circulatory system (*Supplementary Table 20*). PRS for reduced biventricular ejection fraction (PC13) showed strong associations with HF phecodes (OR 1.06, 1.07, $P = 2.74x10^{-8} – 6.19x10^{-7}$), while PRS for reduced annular excursion (PC2) was associated with ischemic and hypertensive phenotypes, despite comprising only two variants (*Supplementary Table 21*).

We also explored relationships between dynamic cardiac shape PC PRS with prevalent and incident cardiometabolic diseases (*Figure 5*). There were seven significant associations between PC PRS and prevalent disease ($P < 0.0083$). Four were associated with prevalent IHD; PC12 (relative left ventricular size) in a risk conferring direction (OR 2.46, CI 1.60-3.78) and PCs 2 (MAPSE/TAPSE), 5 (lateral-septal width, OR 0.45, CI 0.29-0.71) and 6 (left ventricular length, OR 0.75, CI 0.62-0.92) as protective, two with prevalent AF; PCs 6 (LV length) and 10 (right ventricular ejection fraction) (OR 1.73 [CI 1.28-2.37]; OR 1.92 [CI 1.26-2.93]), and one with HF; PC8 (tricuspid valve opening size) (OR 4.71, CI 1.53-14.48) (*Supplementary Table 22*).

Reviewing results from testing of PC PRS with incident disease highlighted that the strongest associations were with incident HF. There were five PC PRS significantly associated with HF: PCs 1 (heart size, OR 1.67, CI 1.36-2.05), 11 (rounder ventricular apex, OR 1.85, CI 1.45-2.36) and 13 (global biventricular ejection fraction, OR 2.05, CI 1.67-2.51) in a risk-conferring direction and PCs 2 (MAPSE/TAPSE, OR 0.41, CI 0.27-0.62) and 3 (ventricular sphericalization, OR 0.76, CI 0.65-0.88) as protective. Four PRS were significantly associated with incident AF; PCs 10 (right ventricular ejection fraction, OR 1.46, CI 1.19-1.79) and 11 (OR 1.48, CI 1.22-1.80) in a risk-conferring direction and PCs 1 (heart size, OR 0.75, CI 0.63-0.88) and 3 (OR 0.66, CI 0.58-0.75) as protective. A full summary of the significant PRS associations can be found in *Supplementary Table 23*.

MR supported a robust causal effect of reduced biventricular ejection fraction (PC13) on HF risk, with consistent estimates across multiple methods (including Inverse variance weighted β 0.492, P $6x10^{-7}$

and Weighted median β 0.408, P 4.2×10^{-5}) and no evidence of horizontal pleiotropy. Additional significant causal relationships were observed with disease as the exposure and dynamic cardiac shape as the outcome (reporting inverse variance weighted results, full results in *Table 4*); between T2D and PCs 1 (overall heart size) (β -0.05, P 0.003) and 12 (relative LV size) (β 0.04, P 0.008); between IHD and PC9 (LV basal systolic excursion) (β -0.06, P 0.008), and between HF and PC14 (relative ventricular size and ejection fraction) (β 0.1, P 0.004) (sensitivity analyses in *Supplementary Table 24*). Full MR results are presented in *Supplementary Tables 25-27*.

Discussion

Quantifying dynamic cardiac shape through statistical shape atlasing provides a complementary framework for studying cardiac disease-morphology relationships. By jointly modeling ventricular geometry at ED and ES, dynamic shape phenotypes capture not only static morphology but also functional deformation during contraction. Previously, we showed that these static shape phenotypes have substantially stronger associations with prevalent cardiometabolic diseases than conventional CMR measures, including ejection fraction, strain, and valve excursions[42]. Here, we identified dynamic shape components that are significantly associated with prevalent and incident cardiometabolic disease, influenced by expression of novel genetic loci, PRS of which are also predictive of incident HF and AF, and which are causal for HF by Mendelian randomization. We also improve prediction of incident IHD when adding PC13 (ejection fraction) to standard CMR measures and covariates versus CMR measures and covariates alone.

The dynamic shape atlas builds directly on previous work based on ED shape alone. As expected, significant correlations were observed between ED and dynamic shape PCs, particularly for components capturing global cardiac size. However, beyond the first PC, many dynamic shape PCs showed only modest phenotypic and genetic correlation with ED PCs, indicating that the inclusion of ES information introduces genuinely new variation related to cardiac function. This is further supported by the observation that all dynamic shape PCs demonstrated some degree of genetic signal in the ED GWAS, while the dynamic atlas substantially increased discovery power. Several dynamic shape PCs captured functional features closely aligned with established clinical metrics. PC2 reflected longitudinal annular motion analogous to MAPSE and TAPSE, while PC13 captured variation resembling biventricular ejection fraction. Despite these similarities, correlations with standard measures were incomplete, indicating that dynamic shape phenotypes encode complementary information about cardiac mechanics that is not fully captured by standard CMR metrics.

Strong associations were observed between both prevalent and incident IHD and several dynamic cardiac shape PCs, particularly those capturing functional variation (PCs 2, 9, 13 and 14). Importantly,

424 the direction of these associations consistently reflected impaired cardiac function, including
425 reduced annular plane systolic excursion (PC2) and reduced biventricular ejection fraction (PC13).
426 This association is also seen in the PRS for PC2, however there is disagreement in the direction of
427 effect between the PC and IHD and the PC PRS and IHD which could be attributed to the low percent
428 heritability explained by the two genome-wide significant variants identified for PC2 (0.5%). While
429 IHD is primarily driven by coronary artery pathology, which is not directly captured by ventricular
430 shape atlases, these findings demonstrate that ventricular geometry and systolic deformation
431 encode meaningful information about IHD risk. There is also evidence that PC2 provides
432 complementary information to CMR measures when predicting incident IHD.

433 Diabetes has long been associated with characteristic patterns of cardiac remodeling, including
434 reduced ventricular volumes, increased myocardial mass, and altered systolic performance[72,73].
435 Consistent with prior studies, we observed significant associations between multiple dynamic shape
436 PCs and prevalent T2D (PCs 1, 2, 8, 12, 13), extending our previous findings based on ED shape
437 alone[41]. Some of these observations are supported by MR, with a significant causal relationship
438 observed between T2D on PCs 1 (overall heart size) and 12 (relative LV size). Importantly, dynamic
439 shape PCs capturing both size and functional variation were associated with T2D, highlighting the
440 importance of systolic remodeling in metabolic heart disease. Associations with incident T2D were
441 also observed for all dynamic shape PCs, as well as between T2D and the PRS for PCs 2 and 11,
442 reinforcing the close link between cardiac morphology and metabolic dysfunction [72,74–77]. Together,
443 these findings support the concept that cardiac shape and function reflect a continuum of metabolic
444 stress and insulin resistance[78–82]. Given the difficulty of directly measuring insulin resistance, dynamic
445 cardiac shape phenotypes may serve as informative imaging-derived biomarkers of subclinical
446 metabolic dysfunction.

447 There were substantial associations observed between cardiac shape PCs and HF in the models using
448 both the PCs and PC PRS. PCs 1-8, 12-14 had significant association with prevalent HF, of which the
449 association between prevalent HF and PC8 (tricuspid valve opening size) is mirrored in the PRS
450 results, suggesting a remodeling effect of HF reflecting in dynamic shape. All PCs were significantly
451 associated with incident HF, relationships that were also observed in PRS for PCs 1, 2, 3, 11 and 13,
452 suggesting that dynamic cardiac shape can predispose future HF events. In testing the causality of
453 these associations in MR, a significant causal effect was observed of HF on PC14 (relative ventricular
454 size and ejection fraction), and of PC13 (ejection fraction) on HF. Importantly, the incomplete
455 correlation between PC13 and imaging-derived ejection fraction suggests that this phenotype
456 captures additional functional information relevant to HF beyond standard measures.

457 Dynamic cardiac shape PCs demonstrated moderate-to-high heritability and yielded substantially
458 more genome-wide significant loci than previous ED shape analysis. In total, 75 loci were identified,
459 with 14 genetic signals being novel for cardiac traits. Importantly, even for PCs closely related to ED
460 morphology, such as overall heart size, the inclusion of systolic information increased the number of
461 associated loci, highlighting the added genetic signal captured by dynamic phenotyping.

462 Several novel loci provided candidate genes with established roles in cardiac development, structure,
463 and function, including pathways related to myocardial architecture and contractile mechanisms. In
464 particular, PCs capturing smaller proportions of total variance, reflecting more localized or functional
465 features, had a higher number of associations with novel loci, whereas PCs explaining larger variance
466 overlapped more strongly with known cardiac structure and function traits. This pattern suggests
467 that dynamic shape atlasing enables the discovery of genetic influences on subtler aspects of cardiac
468 mechanisms that are not well represented by traditional imaging phenotypes.

469 Novel signals for cardiac traits included: rs12494109 identified for PC5 (lateral-septal width), the
470 candidate gene is *Wingless-Type MMTV Integration Site Family, Member 5A*, this is a gene implicated
471 in developmental processes during embryogenesis, associated with congenital right ventricular
472 outflow tract obstruction in autosomal recessive Robinow syndrome[83,84], and mouse models exhibit a
473 double outlet right ventricle, atrioventricular septal defect and left ventricular and pulmonary
474 arterial hypoplasia[85].

475 Two variants, rs32841 identified for PC7 (septal position) with potential candidate gene *Gypsy*
476 *Retrotransposon Integrase 1* and rs12939170 identified for PC8 (tricuspid valve opening size) with
477 candidate gene *Replication Protein A1* had knockout mouse models with abnormal cardiac
478 morphology[86] – knockout mice with *Gypsy Retrotransposon Integrase 1* had abnormal heart shape,
479 and knockout mice with *Replication Protein A1* had increased heart weight.

480 Several additional candidate genes were indicated from gene-burden testing, of these some are
481 known cardiomyopathy genes. One example is *Cysteine And Glycine Rich Protein 3 (CRSP3)*, rare
482 variants in this gene are associated with PC14 (left ventricular size and reduced ejection fraction).
483 This gene encodes a muscle LIM protein which is important for cardiac and skeletal muscle structure
484 and function and is a regulator in sarcomere assembly and contraction[87]. A rare variant was
485 associated in *Vacuolar Protein Sorting 25 Homolog* (*VPS25*), *VPS25* encodes a protein that functions
486 in sorting of ubiquitinated membrane proteins during endocytosis, has mouse models with
487 decreased heart weight and hemorrhaging, and has been associated with frontotemporal
488 dementia[88].

Conclusion

In conclusion, dynamic statistical shape atlasing captures cardiac shape variation across the cardiac cycle together with functional deformation, providing robust and interpretable imaging-derived phenotypes that encapsulate substantially more information from CMR than traditional summary measures. Building on previous ED biventricular atlases, this work demonstrates the added value of incorporating systolic information to define shape components that jointly reflect cardiac morphology and function. These dynamic shape PCs show biologically plausible associations with both prevalent and incident cardiometabolic disease and improve disease prediction when added to standard CMR-derived metrics. In genetic analyses, dynamic shape PCs enhance locus discovery compared with ED shape alone, identifying additional variants, including loci not previously implicated in cardiovascular traits. PRS constructed from these variants were also predictive of cardiometabolic outcomes. Together, these findings establish dynamic cardiac shape atlasing as a powerful and interpretable framework for integrating cardiac structure, function, genetics, and disease risk.

In future work this statistical shape atlasing methodology can be applied to more varied cohorts to explore diseases such as cardiomyopathies which are under-represented in UK Biobank, as well as exploring dynamic shape variation within the population due to factors such as sex, age or ancestry. The capacity for dynamic cardiac shape to predict incident cardiometabolic disease can be further explored with more specific datasets, and leveraging the longitudinal repeat imaging data from UK Biobank to assess the clinical utility of these imaging-derived phenotypes.

Ethics approval

This study complies with the Declaration of Helsinki; the work was covered by the ethical approval for UK Biobank studies from the NHS National Research Ethics Service on 17th June 2011 (Ref 11/NW/0382) and extended on 18 June 2021 (Ref 21/NW/0157) with written informed consent obtained from all participants.

Acknowledgements

This research was conducted using the UK Biobank Resource under Application Number 2964. The work uses data provided by patients and collected by the NHS as part of their care and support. This research used data assets made available by National Safe Haven as part of the Data and Connectivity National Core Study, led by Health Data Research UK in partnership with the Office for National Statistics and funded by UK Research and Innovation (grant ref MC_PC_20029). Copyright © (2022), NHS Digital. Re-used with the permission of the NHS Digital [and/or UK Biobank]. All rights reserved. Barts Charity (G-002346) contributed to fees required to access UK Biobank data [access application #2964]. JR acknowledges funding by the Spanish Ministry of Science and Innovation (MCIN/AEI/10.13039/501100011033) for fellowship RYC2021-031413-I. RB, SEP and PBM acknowledge the support of the National Institute for Health and Care Research (NIHR) Barts Biomedical Research Centre (NIHR203330); a delivery partnership of Barts Health NHS Trust, Queen Mary University of London, St George's University Hospitals NHS Foundation Trust and St George's University of London. WJY acknowledges the NIHR Integrated Academic Training program, which supports his Academic Clinical Lectureship post. KU acknowledges support from a British Heart Foundation 4-year PhD studentship (FS/4yPhD/F/23/34196).

Contributions

R.B., J.R., A.Y., and P.B.M. conceived and designed the experiments, R.B., performed the experiments, R.B., and K.U. performed statistical analysis, R.B., J.R., A.Y., and P.B.M. analysed the data, W.J.Y., J.R., A.Y., and P.B.M. contributed reagents/materials/analysis tools, J.R., A.Y., and P.B.M. jointly supervised the research, R.B., J.R., A.Y., and P.B.M. wrote the paper and W.J.Y and S.E.P. provided critical review of the manuscript.

References

1. Leancă, S. A. *et al.* Cardiac Reverse Remodeling in Ischemic Heart Disease with Novel Therapies for Heart Failure with Reduced Ejection Fraction. *Life Basel Switz.* **13**, (2023).
2. Calvieri, C. *et al.* Left Ventricular Adverse Remodeling in Ischemic Heart Disease: Emerging Cardiac Magnetic Resonance Imaging Biomarkers. *J. Clin. Med.* **12**, (2023).
3. Del Buono, M. G. *et al.* Heart Failure After ST-Elevation Myocardial Infarction: Beyond Left Ventricular Adverse Remodeling. *Curr. Probl. Cardiol.* **48**, 101215 (2023).
4. Bhatt, A. S., Ambrosy, A. P. & Velazquez, E. J. Adverse Remodeling and Reverse Remodeling After Myocardial Infarction. *Curr. Cardiol. Rep.* **19**, 71 (2017).
5. Eskerud, I., Gerdts, E., Larsen, T. H. & Lønnebakken, M. T. Left ventricular hypertrophy contributes to Myocardial Ischemia in Non-obstructive Coronary Artery Disease (the MicroCAD study). *Int. J. Cardiol.* **286**, 1–6 (2019).
6. Khalid, K. *et al.* Correlation of Coronary Artery Disease and Left Ventricular Hypertrophy. *Cureus* **13**, e17550 (2021).
7. Raman, B., Bluemke, D. A., Lüscher, T. F. & Neubauer, S. Long COVID: post-acute sequelae of COVID-19 with a cardiovascular focus. *Eur. Heart J.* **43**, 1157–1172 (2022).
8. Merlo, A. *et al.* Right Ventricular Dysfunction before and after Cardiac Surgery: Prognostic Implications. *J. Clin. Med.* **13**, 1609 (2024).
9. Medrano-Gracia, P. *et al.* Left ventricular shape variation in asymptomatic populations: the multi-ethnic study of atherosclerosis. *J. Cardiovasc. Magn. Reson.* **16**, 56 (2014).
10. Corden, B. *et al.* Relationship between body composition and left ventricular geometry using three dimensional cardiovascular magnetic resonance. *J. Cardiovasc. Magn. Reson.* **18**, 32–32 (2016).
11. Mauger, C. *et al.* Right ventricular shape and function: cardiovascular magnetic resonance reference morphology and biventricular risk factor morphometrics in UK Biobank. *J. Cardiovasc. Magn. Reson.* **21**, 41 (2019).
12. Gilbert, K., Mauger, C., Young, A. A. & Suinesiaputra, A. Artificial Intelligence in Cardiac Imaging With Statistical Atlases of Cardiac Anatomy. *Front. Cardiovasc. Med.* **7**, 102–102 (2020).
13. de Marvao, A., Dawes, T. J. W. & O'Regan, D. P. Artificial Intelligence for Cardiac Imaging-Genetics Research. *Front. Cardiovasc. Med.* **6**, (2020).
14. Mauger, C. A. *et al.* Multi-Ethnic Study of Atherosclerosis: Relationship between Left Ventricular Shape at Cardiac MRI and 10-year Outcomes. *Radiology* 220122–220122 (2022) doi:10.1148/radiol.220122.
15. Harold, S., A., H. G. & A., T. F. Heritability of Blood Pressure and Hemodynamics in African- and European-American Youth. *Hypertension* **41**, 1196–1201 (2003).
16. Bella, J. N. *et al.* Heritability of left ventricular dimensions and mass in American Indians: The Strong Heart Study. *J. Hypertens.* **22**, (2004).
17. Busjahn, C. A. *et al.* Heritability of left ventricular and papillary muscle heart size: a twin study with cardiac magnetic resonance imaging. *Eur. Heart J.* **30**, 1643–1647 (2009).
18. Jin, Y. *et al.* Heritability of left ventricular structure and function in Caucasian families. *Eur. J. Echocardiogr.* **12**, 326–332 (2011).
19. Aung, N. *et al.* Genome-Wide Analysis of Left Ventricular Image-Derived Phenotypes Identifies Fourteen Loci Associated With Cardiac Morphogenesis and Heart Failure Development. *Circulation* **140**, 1318–1330 (2019).
20. Aung, N. *et al.* Genome-wide association analysis reveals insights into the genetic architecture of right ventricular structure and function. *Nat. Genet.* **54**, 783–791 (2022).
21. Aung, N. *et al.* Genome-Wide Analysis of Left Ventricular Maximum Wall Thickness in the UK Biobank Cohort Reveals a Shared Genetic Background With Hypertrophic Cardiomyopathy. *Circ. Genomic Precis. Med.* **16**, e003716–e003716 (2023).
22. Pirruccello, J. P. *et al.* Analysis of cardiac magnetic resonance imaging in 36,000 individuals yields genetic insights into dilated cardiomyopathy. *Nat. Commun.* **11**, (2020).

588 23. Pirruccello, J. P. *et al.* Genetic analysis of right heart structure and function in 40,000 people.
589 *Nat. Genet.* **54**, 792–803 (2022).
590 24. Vukadinovic, M. *et al.* Deep learning-enabled analysis of medical images identifies cardiac
591 sphericity as an early marker of cardiomyopathy and related outcomes. *Med N. Y. N* **4**, 252-
592 262.e3 (2023).
593 25. Lu, C. *et al.* New Genetic Loci Implicated in Cardiac Morphology and Function Using Three-
594 Dimensional Population Phenotyping. *Circ. Genomic Precis. Med.* **18**, e005116 (2025).
595 26. Tadros, R. *et al.* Shared genetic pathways contribute to risk of hypertrophic and dilated
596 cardiomyopathies with opposite directions of effect. *Nat. Genet.* **53**, 128–134 (2021).
597 27. Biddinger, K. J. *et al.* Rare and Common Genetic Variation Underlying the Risk of Hypertrophic
598 Cardiomyopathy in a National Biobank. *JAMA Cardiol.* **7**, 715–722 (2022).
599 28. Zheng, S. L. *et al.* Evaluation of polygenic scores for hypertrophic cardiomyopathy in the general
600 population and across clinical settings. *Nat. Genet.* **57**, 563–571 (2025).
601 29. Soh, C. H., Xiang, R., Takeuchi, F. & Marwick, T. H. Use of Polygenic Risk Score for Prediction of
602 Heart Failure in Cancer Survivors. *JACC CardioOncology* **6**, 714–727 (2024).
603 30. Haller, P. M. *et al.* A Polygenic Risk Score to Predict Incident Heart Failure Across the Spectrum of
604 Cardiovascular Risk. *J. Am. Coll. Cardiol.* **86**, 860–873 (2025).
605 31. Khera, A. V. *et al.* Genome-wide polygenic scores for common diseases identify individuals with
606 risk equivalent to monogenic mutations. *Nat. Genet.* **50**, 1219–1224 (2018).
607 32. Weng, L.-C. *et al.* Genetic Predisposition, Clinical Risk Factor Burden, and Lifetime Risk of Atrial
608 Fibrillation. *Circulation* **137**, 1027–1038 (2018).
609 33. Segan, L. *et al.* Combining polygenic and clinical risk scores in atrial fibrillation risk prediction:
610 Implications for population screening. *Heart Rhythm* **22**, 1906–1914 (2025).
611 34. Läll, K., Mägi, R., Morris, A., Metspalu, A. & Fischer, K. Personalized risk prediction for type 2
612 diabetes: the potential of genetic risk scores. *Genet. Med.* **19**, 322–329 (2017).
613 35. Mars, N. *et al.* Polygenic and clinical risk scores and their impact on age at onset and prediction
614 of cardiometabolic diseases and common cancers. *Nat. Med.* **26**, 549–557 (2020).
615 36. Ning, C. *et al.* Genome-wide association analysis of left ventricular imaging-derived phenotypes
616 identifies 72 risk loci and yields genetic insights into hypertrophic cardiomyopathy. *Nat.*
617 *Commun.* **14**, 7900–7900 (2023).
618 37. Meyer, H. V. *et al.* Genetic and functional insights into the fractal structure of the heart. *Nature*
619 https://doi.org/10.1038/s41586-020-2635-8 (2020) doi:10.1038/s41586-020-2635-8.
620 38. Radhakrishnan, A. *et al.* Cross-modal autoencoder framework learns holistic representations of
621 cardiovascular state. *Nat. Commun.* **14**, 2436 (2023).
622 39. Bonazzola, R. *et al.* Unsupervised ensemble-based phenotyping enhances discoverability of
623 genes related to left-ventricular morphology. *Nat. Mach. Intell.* **6**, 291–306 (2024).
624 40. Ometto, S. *et al.* Hundreds of cardiac MRI traits derived using 3D diffusion autoencoders share a
625 common genetic architecture. 2024.11.04.24316700 Preprint at
626 https://doi.org/10.1101/2024.11.04.24316700 (2025).
627 41. Burns, R. *et al.* Genetic basis of right and left ventricular heart shape. *Nat. Commun.* **15**, 9437
628 (2024).
629 42. Burns, R. *et al.* Relationships between heart shape, function, and disease in 38,858 UK biobank
630 participants. *J. Cardiovasc. Magn. Reson. Off. J. Soc. Cardiovasc. Magn. Reson.* **27**, 101919
631 (2025).
632 43. Sudlow, C. *et al.* UK biobank: an open access resource for identifying the causes of a wide range
633 of complex diseases of middle and old age. *PLoS Med.* **12**, e1001779–e1001779 (2015).
634 44. Bycroft, C. *et al.* The UK Biobank resource with deep phenotyping and genomic data. *Nature* **562**,
635 203–209 (2018).
636 45. Petersen, S. E. *et al.* UK Biobank's cardiovascular magnetic resonance protocol. *J. Cardiovasc.*
637 *Magn. Reson.* **18**, 8–8 (2016).

638 46. Mauger, C. *et al.* An Iterative Diffeomorphic Algorithm for Registration of Subdivision Surfaces:
639 Application to Congenital Heart Disease. in 596–599 (2018). doi:10.1109/EMBC.2018.8512394.
640 47. Goodall, C. Procrustes Methods in the Statistical Analysis of Shape. *J. R. Stat. Soc. Ser. B*
641 *Methodol.* **53**, 285–339 (1991).
642 48. van Buuren, S. & Groothuis-Oudshoorn, K. mice: Multivariate Imputation by Chained Equations
643 in R. *J. Stat. Softw.* **45**, 1–67 (2011).
644 49. Tay, J. K., Narasimhan, B. & Hastie, T. Elastic Net Regularization Paths for All Generalized Linear
645 Models. *J. Stat. Softw.* **106**, 1–31 (2023).
646 50. Friedman, J. H., Hastie, T. & Tibshirani, R. Regularization Paths for Generalized Linear Models via
647 Coordinate Descent. *J. Stat. Softw.* **33**, 1–22 (2010).
648 51. Loh, P.-R. *et al.* Contrasting genetic architectures of schizophrenia and other complex diseases
649 using fast variance-components analysis. *Nat. Genet.* **47**, 1385–1392 (2015).
650 52. Loh, P.-R. *et al.* Efficient Bayesian mixed-model analysis increases association power in large
651 cohorts. *Nat. Genet.* **47**, 284–290 (2015).
652 53. Bulik-Sullivan, B. K. *et al.* LD Score regression distinguishes confounding from polygenicity in
653 genome-wide association studies. *Nat. Genet.* **47**, 291–295 (2015).
654 54. Yang, J., Lee, S. H., Goddard, M. E. & Visscher, P. M. GCTA: a tool for genome-wide complex trait
655 analysis. *Am. J. Hum. Genet.* **88**, 76–82 (2011).
656 55. Ng, P. C. & Henikoff, S. Predicting Deleterious Amino Acid Substitutions. *Genome Res.* **11**, 863–
657 874 (2001).
658 56. Adzhubei, I., Jordan, D. M. & Sunyaev, S. R. Predicting functional effect of human missense
659 mutations using PolyPhen-2. *Curr. Protoc. Hum. Genet.* **Chapter 7**, Unit7.20-Unit7.20 (2013).
660 57. McLaren, W. *et al.* The Ensembl Variant Effect Predictor. *Genome Biol.* **17**, 122–122 (2016).
661 58. Giambartolomei, C. *et al.* Bayesian Test for Colocalisation between Pairs of Genetic Association
662 Studies Using Summary Statistics. *PLOS Genet.* **10**, e1004383–e1004383 (2014).
663 59. Barbeira, A. N. *et al.* Exploring the phenotypic consequences of tissue specific gene expression
664 variation inferred from GWAS summary statistics. *Nat. Commun.* **9**, 1825–1825 (2018).
665 60. Boyle, A. P. *et al.* Annotation of functional variation in personal genomes using RegulomeDB.
666 *Genome Res.* **22**, 1790–1797 (2012).
667 61. Schmitt, A. D. *et al.* A Compendium of Chromatin Contact Maps Reveals Spatially Active Regions
668 in the Human Genome. *Cell Rep.* **17**, 2042–2059 (2016).
669 62. Jung, I. *et al.* A compendium of promoter-centered long-range chromatin interactions in the
670 human genome. *Nat. Genet.* **51**, 1442–1449 (2019).
671 63. Weeks, E. M. *et al.* Leveraging polygenic enrichments of gene features to predict genes
672 underlying complex traits and diseases. *Nat. Genet.* **55**, 1267–1276 (2023).
673 64. Blake, J. A. *et al.* Mouse Genome Database (MGD): Knowledgebase for mouse–human
674 comparative biology. *Nucleic Acids Res.* **49**, D981–D987 (2021).
675 65. Watanabe, K., Taskesen, E., van Bochoven, A. & Posthuma, D. Functional mapping and
676 annotation of genetic associations with FUMA. *Nat. Commun.* **8**, 1826–1826 (2017).
677 66. Mbatchou, J. *et al.* Computationally efficient whole-genome regression for quantitative and
678 binary traits. *Nat. Genet.* **53**, 1097–1103 (2021).
679 67. Buniello, A. *et al.* The NHGRI-EBI GWAS Catalog of published genome-wide association studies,
680 targeted arrays and summary statistics 2019. *Nucleic Acids Res.* **47**, D1005–D1012 (2019).
681 68. Carroll, R. J., Bastarache, L. & Denny, J. C. R PheWAS: data analysis and plotting tools for
682 phenome-wide association studies in the R environment. *Bioinforma. Oxf. Engl.* **30**, 2375–2376
683 (2014).
684 69. Choi, S. W. & O'Reilly, P. F. PRSice-2: Polygenic Risk Score software for biobank-scale data.
685 *GigaScience* **8**, giz082 (2019).
686 70. Hemani, G. *et al.* The MR-Base platform supports systematic causal inference across the human
687 phenome. *eLife* **7**, e34408 (2018).

688 71. Lonsdale, J. *et al.* The Genotype-Tissue Expression (GTEx) project. *Nat. Genet.* **45**, 580–585
689 (2013).
690 72. Jensen, M. T. *et al.* Changes in Cardiac Morphology and Function in Individuals With Diabetes
691 Mellitus. *Circ. Cardiovasc. Imaging* **12**, e009476 (2019).
692 73. Kanamori, H. *et al.* Morphological characteristics in diabetic cardiomyopathy associated with
693 autophagy. *J. Cardiol.* **77**, 30–40 (2021).
694 74. Bertrand, A., Lewis, A., Camps, J., Grau, V. & Rodriguez, B. Multi-modal characterisation of early-
695 stage, subclinical cardiac deterioration in patients with type 2 diabetes. *Cardiovasc. Diabetol.* **23**,
696 371 (2024).
697 75. Devereux, R. B. *et al.* Impact of Diabetes on Cardiac Structure and Function. *Circulation* **101**,
698 2271–2276 (2000).
699 76. Jørgensen, P. G. *et al.* Impact of type 2 diabetes and duration of type 2 diabetes on cardiac
700 structure and function. *Int. J. Cardiol.* **221**, 114–121 (2016).
701 77. Sørensen, M. H. *et al.* Cardiac perfusion, structure, and function in type 2 diabetes mellitus with
702 and without diabetic complications. *Eur. Heart J. - Cardiovasc. Imaging* **21**, 887–895 (2020).
703 78. Witteles, R. M. & Fowler, M. B. Insulin-Resistant Cardiomyopathy. *JACC* **51**, 93–102 (2008).
704 79. Kidambi, S., Kotchen, J., Krishnaswami, S., Grim, C. & Kotchen, T. Cardiovascular correlates of
705 insulin resistance in normotensive and hypertensive African Americans (Hemodynamic
706 correlates of insulin resistance). *Metabolism.* **60**, 835–842 (2011).
707 80. Banerjee, D. *et al.* Insulin Resistance and Risk of Incident Heart Failure. *Circ. Heart Fail.* **6**, 364–
708 370 (2013).
709 81. Fan, Y. *et al.* Primordial Drivers of Diabetes Heart Disease: Comprehensive Insights into Insulin
710 Resistance. *Diabetes Metab. J.* **48**, 19–36 (2024).
711 82. Sevilla-González, M. *et al.* Heterogeneous effects of genetic variants and traits associated with
712 fasting insulin on cardiometabolic outcomes. *Nat. Commun.* **16**, 2569 (2025).
713 83. Schleiffarth, J. R. *et al.* Wnt5a Is Required for Cardiac Outflow Tract Septation in Mice. *Pediatr.*
714 *Res.* **61**, 386–391 (2007).
715 84. Li, P. *et al.* Variants in the Regulatory Region of WNT5A Reduced Risk of Cardiac Conotruncal
716 Malformations in the Chinese Population. *Sci. Rep.* **5**, 13120 (2015).
717 85. Lo, C. Information submitted by the NHLBI Cardiovascular Development Consortium (CvDC),
718 Bench to Bassinet Program (B2B/CvDC). MGI Direct Data Submission (B2B/CvDC)
719 https://doi.org/J:175213 (2011).
720 86. Mouse Genome Informatics and the International Mouse Phenotyping Consortium (IMPC).
721 Obtaining and Loading Phenotype Annotations from the International Mouse Phenotyping
722 Consortium (IMPC) Database. Database Release https://doi.org/J:211773 (2014).
723 87. Vafiadaki, E., Arvanitis, D. A. & Sanoudou, D. Muscle Lim Protein: master regulator of cardiac and
724 skeletal muscle function. *Gene* **566**, 1–7 (2015).
725 88. Handschuh, K. *et al.* ESCRT-II/Vps25 Constrains Digit Number by Endosome-Mediated Selective
726 Modulation of FGF-SHH Signaling. *Cell Rep.* **9**, 674–687 (2014).

727

Main Figures

Figure 1. Study overview

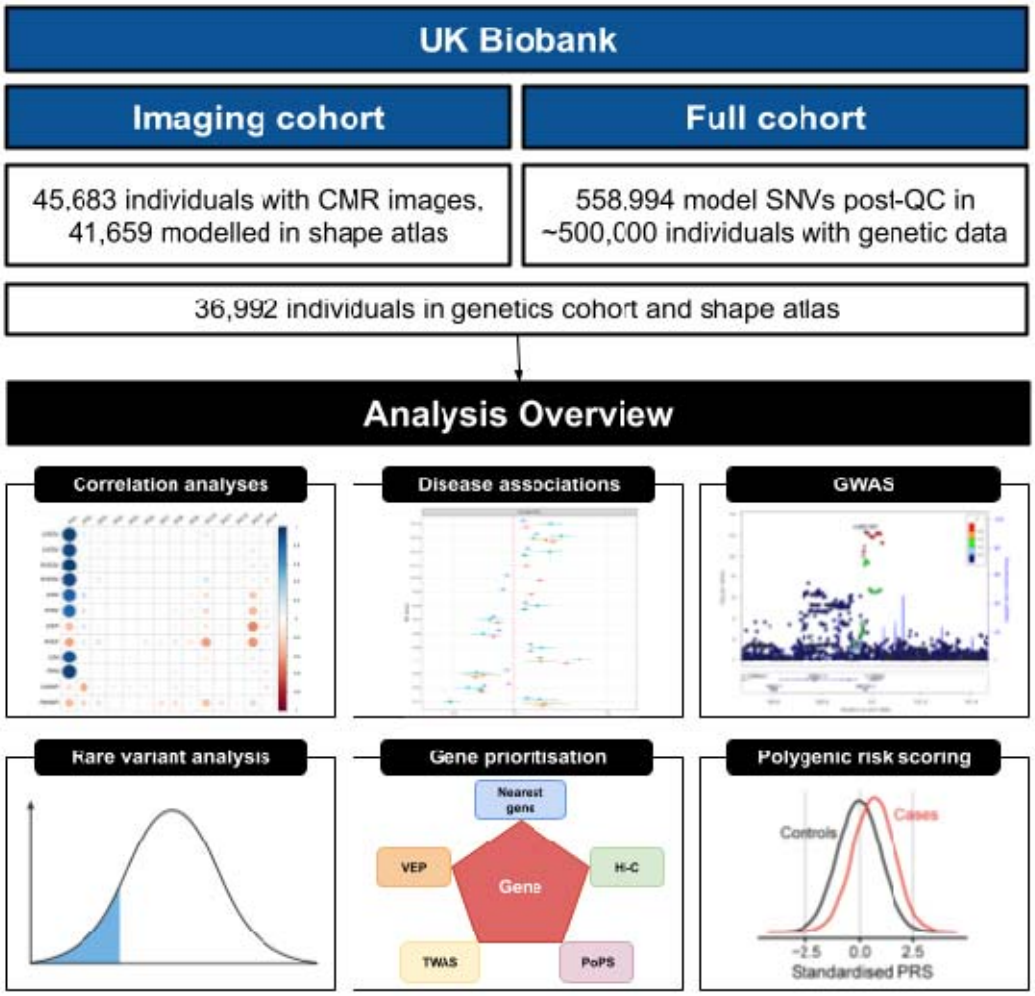

Graphical overview of the study cohorts and analyses performed.

In blue the cohorts used in the imaging and genetics analyses with the sample size for the GWAS indicated. In black there are graphics of the main analyses performed; correlation analyses between dynamic shape PCs and CMR measures, cardiometabolic disease risk factors and end-diastolic PCs; regression analyses between dynamic shape PCs and prevalent and incident cardiometabolic disease; GWAS for dynamic shape PCs; rare variant analysis to identify rare frequency variants associated with dynamic cardiac shape; a gene prioritization bioinformatics pipeline for identifying candidate genes at genome-wide significant loci; polygenic risk scoring and regression analyses to calculate associations between dynamic shape PCs and prevalent and incident cardiometabolic disease.

Abbreviations: CMR, cardiac magnetic resonance (imaging); SNV, single nucleotide variant; QC, quality control; GWAS, genome-wide association study; VEP, variant effect prediction; TWAS, transcriptome-wide association study; PRS, polygenic risk score.

Figure 2. Dynamic shape principal components

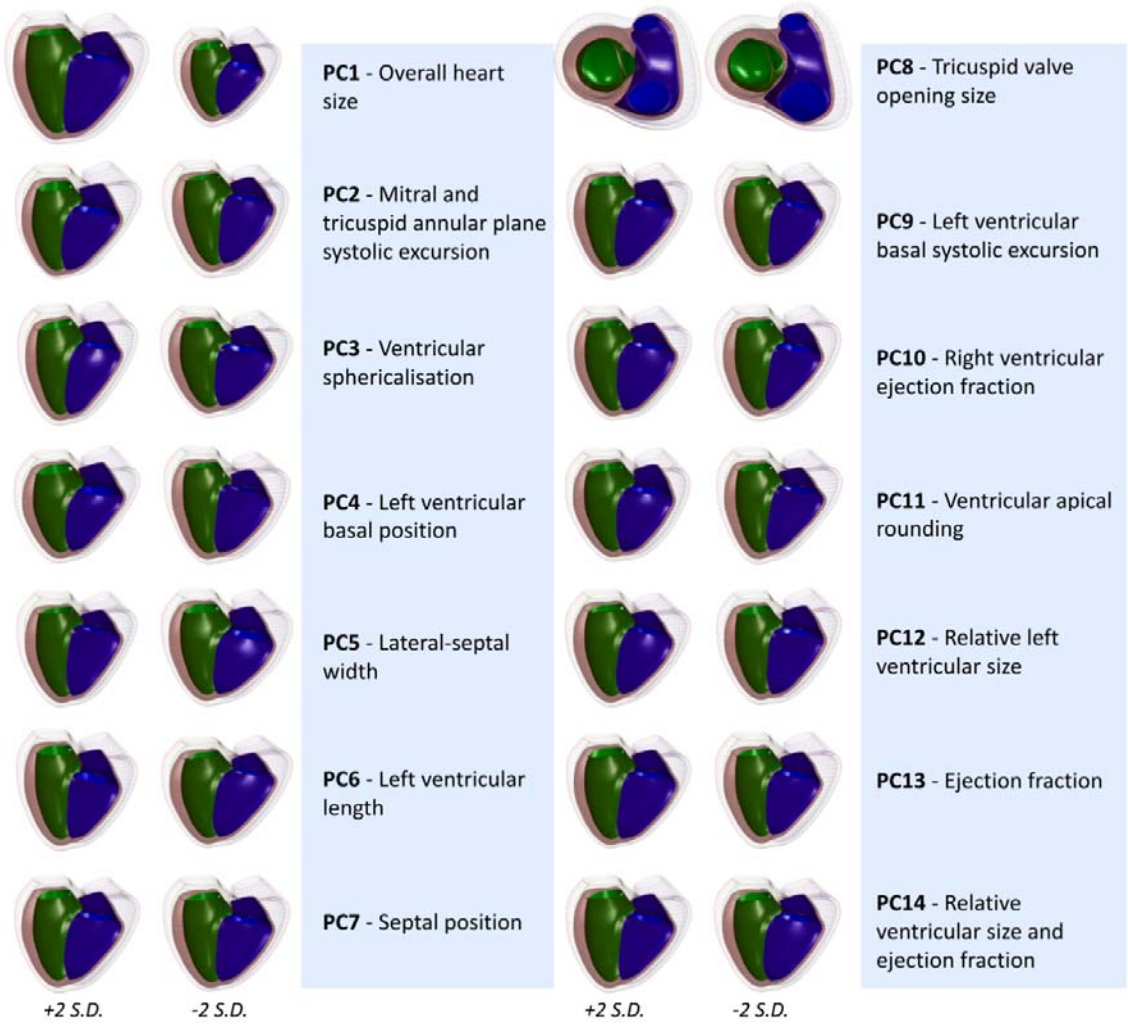

Visual summaries of the dynamic shape variation captured by each PC with a text description.

For each PC, the shape of the biventricular model at ±2 standard deviations from the mean shape in the direction of that PC is represented. Within each biventricular model represented, green indicates the left ventricular endocardium at end-systole, blue indicates the right ventricular endocardium at end-systole, pink indicates the epicardium at end-systole, and these same structures and end-diastole are indicated in wireframe. PC, principal component; S.D., standard deviation.

Figure 3 Disease associations between dynamic cardiac shape and cardiometabolic disease

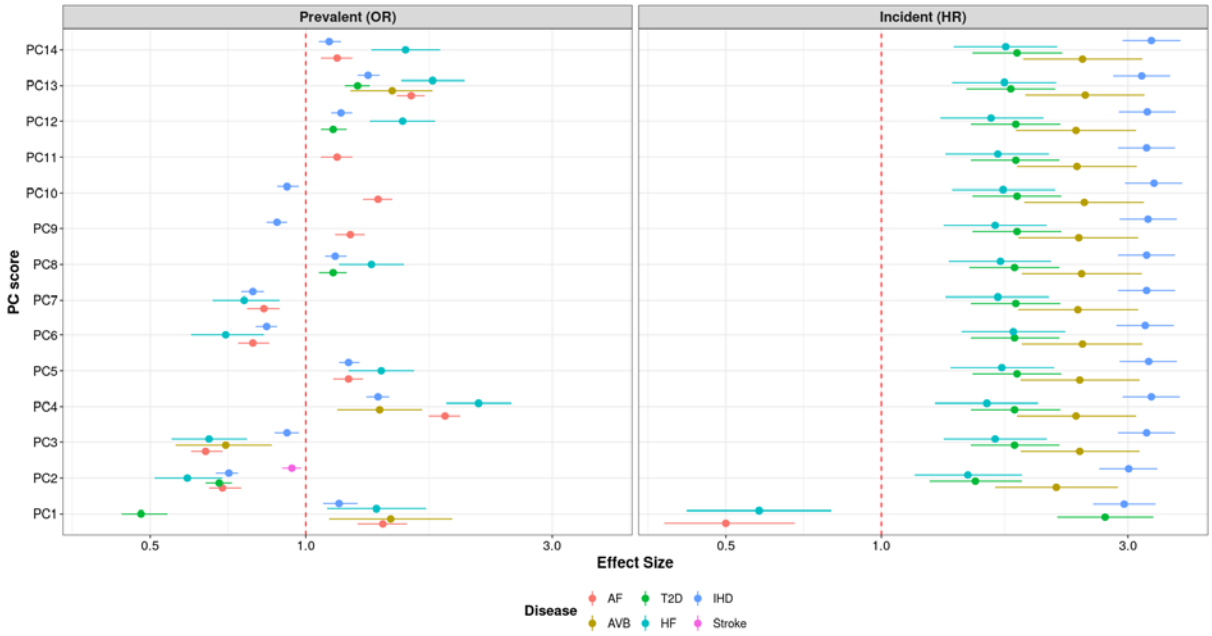

Summary plots of the significant associations between dynamic shape PCs and prevalent and incident cardiometabolic disease.

On the X-axis is the relative effect of change in the PC, represented as odds-ratio for prevalent disease and hazard ratio for incident disease. Each association between PC and disease is color coded, with the effect represented as a dot and the 95% confidence intervals as a line. Only disease associations which are significant (Bonferroni corrected P value < 0.05/6) are shown. The dashed red line on the X-axis represents no effect.

Abbreviations: OR, odds ratio; HR, hazard ratio; AF, atrial fibrillation; AVB, significant 2nd or 3rd degree atrioventricular block; HF, heart failure; T2D, type 2 diabetes mellitus; IHD, ischemic heart disease; PC, principal component; PRS, polygenic risk score.

Figure 4. Circos plot of GWAS results and associations with CMR measures

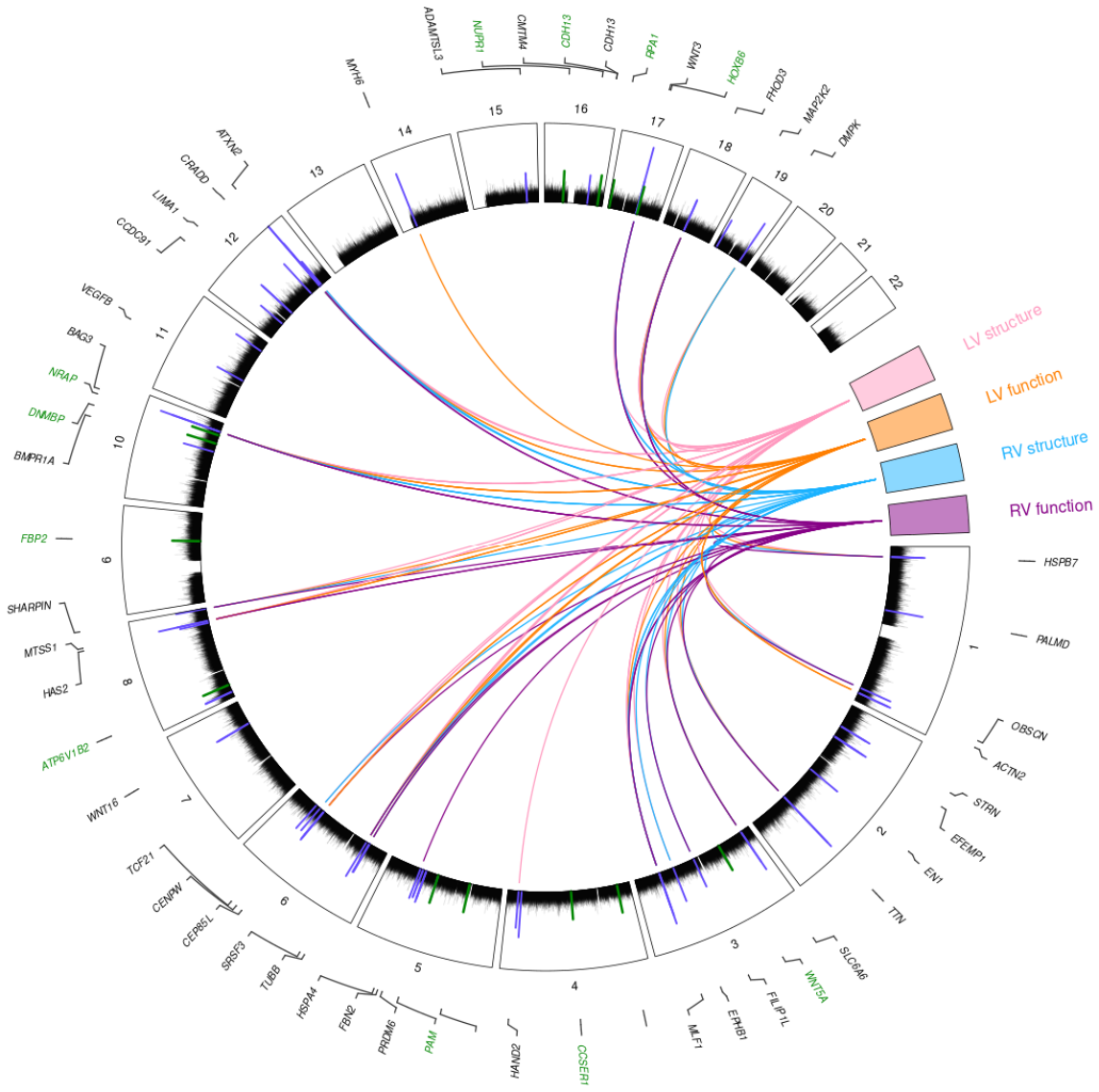

A circos plot summarizing the genetic basis of dynamic cardiac shape.

Visualized is a circular Manhattan plot with genome-wide association study summary statistics for each of the 14 dynamic shape principal components overlaid. Chromosomes are divided into segments numbered on the outside of the Manhattan plot; genomic position is along the X-axis and Log10 P-Value on the Y-axis. The genome-wide significant variants ($P \leq 5x10^{-8}$) which have been previously reported for CMR ventricular structural and functional traits are highlighted in blue, and genome-wide significant variants which have not been previously identified for any cardiovascular-related trait (n=14) are highlighted in green. For each genome-wide significant variant, the candidate gene annotated by the PoPS tool is indicated on the outside of the plot with a line pointing to the variant position. The plot also illustrates genome-wide significant variants which have been identified previously for CMR structural and functional measures; divided into left and right ventricular structural and functional CMR measures. These have segments in the plot alongside the chromosomes, color coded with lines leading to the significant variants that have been associated with the trait. LV, left ventricular; RV, right ventricular.

Figure 5 Disease associations between dynamic cardiac shape polygenic risk scores and cardiometabolic disease

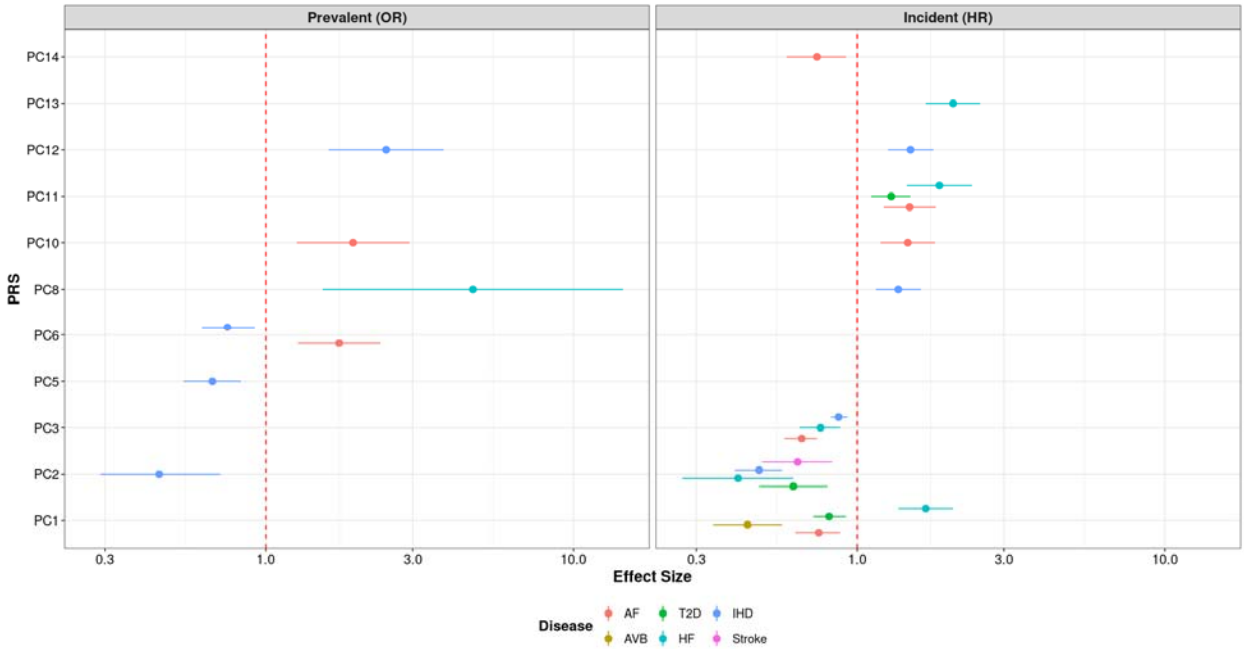

Summary plots of the significant associations between dynamic shape PC PRS and prevalent and incident cardiometabolic disease.

On the X-axis is the relative effect of change in the PC PRS, represented as odds-ratio for prevalent disease and hazard ratio for incident disease. Each association between PC PRS and disease is color coded, with the effect represented as a dot and the 95% confidence intervals as a line. Only disease associations which are significant (Bonferroni corrected P value < 0.05/6) are shown. The dashed red line on the X-axis represents no effect.

Abbreviations: OR, odds ratio; HR, hazard ratio; AF, atrial fibrillation; AVB, significant 2nd or 3rd degree atrioventricular block; HF, heart failure; T2D, type 2 diabetes mellitus; IHD, ischemic heart disease; PC, principal component; PRS, polygenic risk score.

Main Tables

Table 1. Study demographics of the imaging and full cohorts in UK Biobank

Trait	Imaging *N = 41,056*	Full cohort *N = 487,284*
Age, years	55.0 (7.6)	56.5 (8.1)
Male sex	21,366 (52.0%)	264,700 (54.2%)
Height, cm	169.6 (9.2)	168.5 (9.3)
Body mass index, kg/m^2	26.5 (4.2)	27.4 (4.8)
Systolic Blood pressure*, mmHg	138.9 (20.4)	142.9 (21.8)
Diastolic Blood pressure*, mmHg	82.7 (11.4)	84.3 (11.9)
Previous or current smoker	16,205 (39.5%)	220,084 (45.1%)
Regular alcohol use (≥3 times per week)	20,882 (50.1)	212,026 (43.4)
Serum LDL levels*, mmol/l	*NA*	3.8 (0.9)
Serum HDL levels*, mmol/l	*NA*	1.4 (0.4)
Serum triglyceride levels*, mmol/l	*NA*	1.75 (1.0)
Genetically inferred ancestry		
European	38,767	459,783
African	241	7,823
South Asian	455	9,731
East Asian	145	2,115
Cardiometabolic disease		
Ischemic heart disease†	6,066 (14.77, 39.56)	121,299 (24.89, 24.05)
Heart failure†	526 (1.28, 66.73)	18,384 (3.77, 10.19)
Type 2 diabetes†	2,283 (5.56, 40.21)	58,782 (12.06, 21.72)
Significant atrioventricular block†	407 (0.99, 73.46)	11,101 (2.28, 9.37)
Atrial fibrillation†	1,446 (3.52, 34.02)	31,208 (6.40, 19.79)
Stroke†	4,109 (10.00, 27.43)	65,913 (13.53, 36.43)
CMR measures		
RVEDV, ml	148.5 (35.3)	
RVESV, ml	66.6 (20.7)	
RVSV, ml	81.9 (19.7)	
RVEF, %	55.5 (7.2)	
LVEDV, ml	147.9 (33.7)	
LVESV, ml	68.9 (19.7)	
LVM, g	124.2 (26.7)	
LVSV, ml	79.0 (18.4)	
LVEF, %	53.7 (6.2)	

*Numbers are mean (standard deviation) or total number (%). *Systolic and diastolic blood pressure were adjusted for anti-hypertensive medication use by adding 15mmHg and 10mmHg, respectively. † Diseases are reported as total number of cases available in UK Biobank cohort, with the percentage of the total respective UKB cohort that are case positive and the percentage of those cases that are incident (diagnosed after the respective visit - baseline visit for the genetics cohort excluding the imaging cohort, and imaging visit for the imaging cohort) in brackets. Abbreviations: RVEDV, right ventricular end-diastolic volume; RVESV, right ventricular end-systolic volume; RVSV, right ventricular stroke volume; RVEF, right ventricular ejection fraction; LVEDV, left ventricular end-diastolic volume; LVESV, left ventricular end-systolic volume; LVSV, left ventricular stroke volume; LVEF, left ventricular ejection fraction; bpm, beats per minute (heart).*

Table 2. Summary of dynamic shape PCs

PC	Biological feature	Variation direction (Higher/Lower)		Variance explained (%)
		Higher	Lower	
1	Overall heart size	Bigger heart	Smaller heart	34.07
2	Mitral and tricuspid annular plane systolic excursion	Greater degree of MAPSE/TAPSE	Lesser degree of MAPSE/TAPSE	10.62
3	Ventricular sphericalisation	Thinner and longer ventricles	Shorter and wider ventricles in anterior posterior direction	7.81
4	Left ventricular basal position	Lower mitral plane and wider RV in anterior-posterior direction	Higher mitral plane and higher angled tricuspid valve plane	5.52
5	Lateral-septal width	Narrower in the lateral septal direction	Wider in lateral septal direction	5.46
6	Left ventricular length	Longer LV length	Shorter LV length	4.22
7	Septal position	Septal position more shifted to the left	Septal position more shifted towards the right	4.02
8	Tricuspid valve opening size	Smaller tricuspid valve opening	Wider tricuspid valve opening	2.41
9	LV basal systolic excursion	Reduced MAPSE	Greater MAPSE	2.08
10	Right ventricular ejection fraction	Greater RV ejection fraction	Less RV ejection fraction	2
11	Rounder ventricular apex	Rounder apex of the ventricles	More elongated and pointed ventricular apex	1.6
12	Relative left ventricular size	Greater relative size of the LV	Smaller LV relative to the RV	1.3
13	Ejection fraction	Reduced LV and RV ejection fraction	Greater LV and RV ejection fraction	1.14
14	Relative ventricular size and ejection fraction	smaller RV, with reduced LV ejection fraction	Larger RV, greater LV ejection fraction	1.04

Abbreviations: PC, principal component; LV, left ventricle; RV, right ventricle; TAPSE, tricuspid (valve) annular plane systolic excursion.

Table 3. Lead genetic variants and secondary signals from genome-wide association study

PC	Nearest gene	Lead variant	CHR	Position (Hg19)	EA	NEA	MAF	BETA	SE	P value
1	*ATXN2*	rs653178	12	112007756	C	T	0.481	-0.037	0.004	2.70E-21
1	*TTN*	rs2042995	2	179558366	T	C	0.223	0.042	0.005	1.30E-18
1	*BAG3*	rs72840788	10	121415685	G	A	0.218	0.041	0.005	3.40E-17
1	*RSPH6A*	rs7257103	19	46306904	C	T	0.344	-0.03	0.004	1.30E-12
1	*LSM3*	rs73028849	3	14272766	G	C	0.34	0.026	0.004	2.90E-10
1	*EPHB1*	rs77709005	3	134444297	C	T	0.148	0.035	0.006	4.00E-10
1	*MLF1*	rs9810339	3	158302517	T	C	0.496	-0.025	0.004	4.30E-10
1	*GOSR2*	rs533030436	17	45091770	A	G	0.12	-0.038	0.006	2.20E-09
1	*OBSCN*	rs78529941	1	228551488	G	A	0.38	-0.024	0.004	3.00E-09
1	*HLA-DRB5*	rs6939900	6	31228357	C	T	0.357	0.025	0.004	3.00E-09
1	*FHOD3*	rs2644262	18	34223566	T	C	0.271	0.026	0.004	3.80E-09
1	*LINC00964*	rs34123659	8	125862029	T	TA	0.186	0.03	0.005	4.90E-09
1	*CLCNKA*	rs28579893	1	16347534	A	G	0.327	-0.024	0.004	5.20E-09
1	*HSPA4*	5:132409975_CT_C	5	132409975	CT	C	0.267	0.027	0.005	5.90E-09
1	*PLEC*	rs11786896	8	145018354	C	T	0.051	0.052	0.009	1.10E-08
1	*PLCB3*	rs71468663	11	64018104	A	AC	0.047	0.052	0.009	2.20E-08
1	*CENPW*	rs373980643	6	126699611	GT	G	0.457	-0.022	0.004	2.50E-08
2	*EFEMP1*	rs3791679	2	56096892	A	G	0.228	-0.046	0.008	1.20E-09
2	*PTPN11*	rs11066320	12	112906415	A	G	0.423	-0.037	0.006	7.40E-09
3	*PALMD*	rs1890753	1	100039519	G	C	0.478	0.043	0.007	1.00E-10
3	*EN1*	rs332659	2	119456238	A	C	0.326	0.044	0.007	5.30E-10
3	*PALLD*	rs10155248	4	169666162	T	A	0.474	-0.048	0.007	9.40E-13
3	*PRDM6*	rs10077410	5	122450771	G	A	0.136	0.054	0.01	2.30E-08
3	*CDKN1A*	rs3176326	6	36647289	G	A	0.199	-0.055	0.008	8.30E-11
3	*DNMBP**	rs11190360	10	101760736	T	C	0.058	-0.082	0.014	1.30E-08
3	*NRAP**	rs10749139	10	115415214	T	C	0.137	-0.055	0.01	3.80E-08
3	*DIP2B*	rs112716157	12	50907656	C	CA	0.414	0.051	0.007	1.30E-11
3	*CRADD*	rs4144499	12	94151844	C	T	0.496	-0.044	0.007	3.20E-11
3	*GOSR2*	rs17608766	17	45013271	T	C	0.145	0.084	0.009	1.30E-18
3	*MIR196A1**	rs71366902	17	46719157	A	AT	0.206	0.045	0.008	4.20E-08
4	*PRDM6*	rs186749	5	122454305	A	G	0.356	0.039	0.007	2.00E-08
5	*WNT5A**	rs12494109	3	55491571	C	A	0.456	0.038	0.007	4.70E-08
5	*HAND2-AS1*	rs12502027	4	174600223	A	G	0.362	-0.046	0.007	2.40E-10
5	*PRDM6*	rs398028	5	122454550	C	T	0.203	-0.052	0.009	2.20E-09
5	*HLA-DRB5*	rs2284174	6	30713580	T	C	0.224	-0.05	0.008	2.90E-09
5	*HLA-DRB5*	6:31588020_CCTCT_C	6	31588020	CCTCT	C	0.362	0.043	0.007	3.30E-09
5	*CCDC91*	rs2638950	12	28551567	A	G	0.244	0.044	0.008	4.30E-08
5	*ADAMTSL3*	rs6602994	15	84490757	T	C	0.279	0.043	0.008	2.20E-08
6	*EFEMP1*	rs201699038	2	56075676	AT	A	0.156	0.06	0.009	1.30E-10
6	*RSRC1*	rs11710570	3	158056654	T	C	0.448	0.052	0.007	1.00E-14
6	*CEP85L*	rs11756440	6	118993642	C	A	0.473	0.041	0.007	8.00E-10
6	*TCF21*	rs162185	6	134226147	T	C	0.409	-0.039	0.007	9.80E-09

6	*FAM3C*	rs12531355	7	121027434	C	T	0.271	0.048	0.008	2.00E-10
6	*HAS2-AS1*	rs62526480	8	122681022	T	C	0.406	-0.038	0.007	2.00E-08
6	*DDX6**	rs12223220	11	118587888	A	G	0.175	-0.053	0.009	1.10E-08
6	*ZBTB7A*	rs66534382	19	4056366	G	A	0.19	0.049	0.009	9.70E-09
7	*HEATR1*	rs531997	1	236803402	A	G	0.179	-0.053	0.009	3.00E-09
7	*PPIP5K2**	rs32841	5	102478258	A	G	0.347	0.041	0.007	2.40E-08
7	*TBX3*	rs10850409	12	115381740	G	A	0.268	0.044	0.008	1.30E-08
8	*SGF29**	rs151091024	16	28569054	A	G	0.026	-0.13	0.022	6.40E-09
8	*DPH1**	rs12939170	17	1937526	C	T	0.028	-0.115	0.021	4.60E-08
9	*SLIT2**	rs6821503	4	19609401	C	T	0.263	0.042	0.008	3.90E-08
9	*LZTS1-AS1**	rs7014186	8	20318812	A	C	0.115	-0.057	0.01	4.30E-08
9	*MFSD14B**	9:97209762_TG_T	9	97209762	TG	T	0.108	-0.076	0.014	4.40E-08
10	*MYH6*	rs422068	14	23864804	T	C	0.356	-0.057	0.007	1.50E-15
10	*FHOD3*	18:34219777_G_GTT	18	34219777	G	GTT	0.248	0.048	0.008	1.80E-09
10	*BAG3*	rs17617337	10	121426884	C	T	0.218	0.047	0.008	9.70E-09
10	*CMTM4*	16:66690988_AT_A	16	66690988	AT	A	0.489	-0.039	0.007	2.30E-08
11	*CDKN1A*	rs3176326	6	36647289	G	A	0.199	0.058	0.009	4.20E-11
11	*STRN*	rs138934670	2	37136145	A	AAAC	0.356	0.048	0.008	1.50E-09
11	*CDH13**	rs9932314	16	82881172	C	T	0.498	0.04	0.007	1.00E-08
11	*ITGA1**	rs60757101	5	51603171	T	A	0.168	-0.056	0.01	2.50E-08
11	*CCSER1**	rs77504602	4	92260138	C	A	0.288	-0.042	0.008	4.40E-08
12	*FBN2*	rs13185878	5	127962298	A	G	0.273	-0.043	0.008	1.90E-08
12	*HEATR5B*	rs1105014	2	37265727	G	C	0.479	-0.038	0.007	2.10E-08
13	*BAG3*	rs2234962	10	121429633	T	C	0.218	0.061	0.008	4.60E-14
13	*LINC00964*	rs34866937	8	125859850	G	A	0.314	0.054	0.007	5.90E-14
13	*LSM3*	rs56242556	3	14273472	C	T	0.215	-0.058	0.008	1.30E-12
13	*HSPB7**	rs1048238	1	16341649	C	T	0.428	-0.041	0.007	1.30E-09
13	*LDB3*	rs35605324	10	88443703	G	A	0.081	0.071	0.012	6.60E-09
13	*FAM86B3P*	rs1915986	8	8114543	A	G	0.499	0.038	0.007	2.10E-08
14	*SLC35F1*	rs17079881	6	118566187	A	G	0.134	0.063	0.01	2.90E-10
14	*ACTN2*	rs12724121	1	236852282	A	T	0.371	-0.044	0.007	6.70E-10
14	*CMSS1*	rs12488245	3	99835254	T	C	0.416	-0.04	0.007	1.00E-08
14	*FHOD3*	18:34219777_G_GTT	18	34219777	G	GTT	0.248	0.044	0.008	4.00E-08
Conditionally independent secondary signals										
1	*SLC6A6*	rs34234056	3	14418444	A	G	0.494	0.021	0.004	1.10E-07
11	*CDH13*	rs4366697	16	83067983	G	C	0.322	0.038	0.007	2.80E-07

Abbreviations: PC, Principal component; CHR, chromosome; Hg19, Genome Reference Consortium Human Build 37 (GRCh37); EA, effect allele; NEA, non-effect allele; Beta, effect size; SE, standard error; p, probability value.

** indicates variant not previously reported for a cardiac trait.*

Table 4. Significant Mendelian Randomization results

Exposure	Outcome	Method	n SNV	Beta	SE	P value	MR Egger Het P	Inverse variance weighted Het P	Pleiotropy P
PC13	HF	Inverse variance weighted	5	0.49	0.10	6.00E-07	0.04	0.08	0.86
PC13	HF	Weighted median	5	0.41	0.10	4.18E-05	0.04	0.08	0.86
T2D	PC12	Inverse variance weighted	138	0.04	0.01	0.008	0.01	0.01	0.28
T2D	PC12	Weighted median	138	0.07	0.02	3.64E-04	0.01	0.01	0.28
T2D	PC12	Weighted mode	138	0.09	0.03	0.001	0.01	0.01	0.28
T2D	PC1	Weighted mode	154	-0.05	0.02	0.003	<1E-7	<1E-7	0.14
HF	PC14	Inverse variance weighted	37	0.10	0.04	0.004	0.05	0.05	0.36
IHD	PC9	Inverse variance weighted	175	-0.06	0.02	0.008	0.20	0.21	0.75

Abbreviations: PC, principal component; T2D, type 2 diabetes mellitus; HF, heart failure; IHD, ischemic heart disease; SNV, single nucleotide variants included in analysis; SE, standard error.